Ocean Science Journal
https://doi.org/10.1007/s12601-021-00049-5

Online ISSN 2005-7172
Print ISSN 1738-5261

ARTICLE

Impact of Different Wind Representations on Resonant Ocean Near-inertial Motions in the Gulf of Mexico

Chuan-Yuan Hsu[1] · Jongsun Kim[1,4] · Ping Chang[1,2] · Steven F. DiMarco[1,3]

Received: 8 March 2021 / Revised: 5 July 2021 / Accepted: 10 October 2021

Abstract
This study investigates the resonated diurnal impact of the surface wind forcing from several atmospheric wind products, including CCMP (Cross-Calibrated Multi-Platform), ERA Interim, NCEP-2 (NCEP-DOE AMIP-II Reanalysis), MERRA (Modern-Era Retrospective analysis for Research and Application), NARR (Northern American Regional Reanalysis) and NAM (North American Mesoscale Forecast System), on the wind-driven near-inertial ocean motions in the northern Gulf of Mexico by numerical simulation, and in comparison, with NDBC buoy surface observed winds. Our analyses show that the near-inertial wind power input, which can affect vertical mixing in the water column, is closely associated with the variability of land-sea breeze by various wind products. In comparison with buoy observations in the northern Gulf of Mexico, the MERRA has the worst land-sea breeze representation, while the NCEP2 and CCMP, which are chosen to represent the coarsest and medium–high horizontal resolution, have the best performance. We further show that by comparison of the buoy data, that the near-inertial wind power input derived from all the wind products is underestimated by 30–50% approximately.

Keywords Gulf of Mexico · Land–sea breeze · Numerical simulation · Oceanic near-inertial waves

1 Introduction

Near-inertial waves excited by wind stress at the ocean surface have long been recognized as an important source of ocean kinetic energy (Munk 1980). About 75–85% of power input is estimated to dissipate within the upper ocean (~200 m) due to the enhanced vertical shear at the bottom of the mixed layer (Furuichi et al. 2008; Zhai et al. 2009), elevating mixing levels in the upper water column and cooling the sea surface temperature. This further may influence the climate through air-sea heat fluxes and atmospheric teleconnections (Jochum et al. 2013).

✉ Chuan-Yuan Hsu
chsu1@tamu.edu

[1] Department of Oceanography, Texas A&M University, College Station, TX 77843-3146, USA

[2] Department of Atmospheric Science, Texas A&M University, College Station, TX 77843-3146, USA

[3] Geochemical and Environmental Research Group, Texas A&M University, College Station, TX 77843-3149, USA

[4] Graduate School of Oceanography, University of Rhode Island, Narragansett, RI 02882, USA

Wind power input to near-inertial motions in the ocean is estimated to be in the range of 0.5–1.4 TW (e.g., Wunsch 1998; Watanabe and Hibiya 2002; Alford 2003a, b; Jiang et al. 2005; Rimac et al. 2013). The large variation in the estimate results is mostly due to the uncertainty in winds that are responsible for generating near-inertial (NI) motions. It is found that the wind power input tends to increase with increasing spatial and temporal resolutions of wind products (e.g., Klein et al. 2004; Jiang et al. 2005; von Storch et al. 2007 and 2012, Rimac et al. 2013). For instance, Rimac et al. (2013) calculated the power input using a global eddy-resolving ocean model forced by NCEP Climate Forecast System Reanalysis (CSFR; Saha et al. 2010) wind stresses subsampled at different resolutions and showed that the wind power input increases from 0.3 TW for low-resolution (6 hourly, 1.875°) wind stresses to 1.1 TW for high-resolution wind stresses (1 hourly, 0.35°).

Most of the NI oscillations are generated during the passage of atmospheric fronts, winter storms, and tropical cyclones/hurricanes. However, near the critical latitude (30°), NI motions can be also generated by the resonance between atmospheric diurnal circulations and local inertial oscillations due to the coincidence between the inertial

Published online: 29 November 2021

frequency and diurnal frequency (Craig 1989a, b). Literatures have demonstrated that the resonant ocean response can be found in New York Bight (Hunter et al. 2007), the Georgia Bight (Edwards 2008), the Southern California Bight (Nam and Send 2013), the Namibian shelf (Hyder et al. 2011; Simpson et al. 2002), and the Catalonian shelf (Rippeth et al. 2002). In addition, such ocean response plays a dominant role in generating NI motions in the Northern Gulf of Mexico around the critical latitude where diurnal wind variation is strong in summer due to the presence of land-sea breeze (LSB) circulation (Simpson et al. 2002; Zhang et al. 2009). Teague et al. (2014) pointed out that inertial currents can be easily enhanced during summer by phase-locking with LSB to reach a speed over 20 cm s^{-1}.

The Northern Gulf of Mexico has been extensively studied using ocean model simulations forced by various wind products [CCMP/NCEP GFS winds: Xu et al. 2013; COADS (Comprehensive Ocean–Atmosphere Dataset) winds: Morey et al. 2005; Zavala-Hidalgo et al. 2003; NARR winds: Feng et al. 2014; Zhang and Hetland 2012; NCEP winds: Cardona and Bracco 2016]. However, differences among these wind products in representing the LSB and their immediate influences on simulated oceanic NI motions have not been systematically evaluated. Given the close associations between surface wind forcing and NI motions, it is of interests to evaluate how well the diurnal variability of these wind datasets compares to that of buoy observation and its impact on the modeled NI motions over the Northern Gulf of Mexico. In this study, we assess the representation of diurnal winds in several widely used wind products, and their impact on simulating NI motions based on an eddy-resolving regional ocean model. A brief description of the ocean model and model experiments is illustrated in Sect. 2. A systematic assessment for various wind products is detailed in Sect. 3. The conclusions and discussions of the study are summarized in Sect. 4.

2 Data and Methods

2.1 Surface Wind Data

Several widely use of gridded 10 m wind products are exanimated in this study (Table 1), including Cross-Calibrated Multi-Platform (CCMP; https://climatedataguide.ucar.edu/climate-data/ccmp-cross-calibrated-multi-platform-wind-vector-analysis; Atlas et al. 2011), ERA Interim (ERAi, https://www.ecmwf.int/en/forecasts/datasets/reanalysis-datasets/era-interim; Dee et al. 2011), Modern-Era Retrospective analysis for Research and Application reanalysis (MERRA, https://gmao.gsfc.nasa.gov/reanalysis/MERRA/; Rienecker et al. 2011), NCEP Atmospheric Model Intercomparison Project Reanalysis (NCEP2, https://www.esrl.noaa.gov/psd/data/gridded/data.ncep.reanalysis2.html; Kanamitsu et al. 2002), NCEP North American Regional Reanalysis (NARR https://www.esrl.noaa.gov/psd/data/gridded/data.narr.html; Mesinger et al. 2006), and North American Mesoscale System (NAM, https://www.ncdc.noaa.gov/data-access/model-data/model-datasets/north-american-mesoscale-forecast-system-nam; Rogers et al. 2009). The NCEP2 is chosen to represent the coarse resolution; the MERRA, ERAi and CCMP are chosen to represent medium–high horizontal resolutions; the NARR and NAM are chosen to represent high horizontal resolutions. All these gridded wind products are on a reanalysis level except NAM, which is a forecast product.

The observational wind dataset used for validating the reanalysis winds was obtained from the National Data Buoy Center (NDBC). This dataset provides continuous wind measurements at various buoy stations over the Gulf of Mexico. However, the wind is measured at different height with different time stamps (e.g., 5, 10 or 30 min) at different stations. To facilitate comparisons with the reanalysis winds, the observed winds were all converted to the standard height

Table 1 Parameters of the wind dataset used in this study

Acronym	Name of Product	Grid resolution	Time resolution
CCMP	Cross-Calibrated Multi-Platform Ocean Surface Wind Dataset	0.25° × 0.25°	4 times daily
ERAi	ECMWF ERA Interim	0.75° × 0.75°	4 times daily
MERRA	Modern-Era Retrospective analysis for Research and Application reanalysis	0.667° × 0.5°	24 times daily
NCEP2	NCEP-DOE reanalysis 2	1.875° × 1.875°	4 times daily
NARR	NCEP North American Regional Reanalysis	32 km × 32 km	8 times daily
NAM	North American Mesoscale System	12 km × 12 km	3 hourly forecast, 4 times daily

of 10 m above the sea surface based on the neutral wind conversion by Large and Pond (1981).

It should be noted that the temporal resolution differs among different products. Therefore, differences in simulated NI waves by various wind products can come from either the accuracy of the products in representing the LSB or/and the sampling frequency of the datasets. The influence of the latter on simulated NIOs has been well studied (Klein et al. 2004; Rimac et al. 2013) and an analytical expression for the influence was derived (Jing et al. 2015). Therefore, we focus on the former effect in this study. To eliminate the sampling frequency effect, we subsampled all the wind products onto the same 6 h interval so that the temporal resolution for all the wind products is identical.

2.2 Near-Inertial Wind Power Input

Near Inertial (NI) I Wind Power Input (WPI) is the dot product of wind stress and surface velocity vector within near-inertial band. To introduce the NI WPI, a commonly used damped slab ocean model will be introduced here. The slab ocean model describes a simple dynamical mixed layer model of a constant depth with linear Ekman dynamics, and the use of a slab ocean model (Pollard and Millard 1970; D'Asaro 1985; Alford 2003a; Mickett et al. 2010) provides an analytically tractable way to study the generation of near-inertial oscillations by surface winds. This simple modeling analysis assumes that (1) nonlinear advective processes are negligibly small, (2) near-surface currents are vertically uniform within the surface mixed layer, (3) wind stresses vanish at the mixed-layer base, (4) vertical mixing is negligible and (5) downward radiation of near-inertial energy through the pressure term can be parameterized as a linear damping term. Under these assumptions, the horizontal momentum equation within the slab ocean model can be written as:

$$\frac{dZ}{dt} + (r + if)Z = \frac{T}{H}, \tag{1}$$

where $Z = u + iv$ is the mixed layer currents; $T = \rho^{-1}\left(\tau_x + i\tau_y\right)$ indicates the 10 m wind stress; *ρ is the air density;*τ_x, τ_y *indicate the wind stress on x, y directions; H* is the mixed-layer depth (MLD); f is the local inertial frequency; r is a tunable damping coefficient representing the radiational decay by downward propagation of near-inertial waves, and can be written as,

$$r(\sigma) = r_o\left(1 - e^{-\frac{\sigma^2}{2\sigma_c^2}}\right), \tag{2}$$

where$r_o = 0.15f, \sigma$ *is the rotary frequency and* $\sigma_c \equiv f/2$ (Alford 2003a, b). The wind stress is estimated based on Donelan et al. (2010). The MLD is fixed at the climatological summer value for simplicity as previous studies (Alford 2001) suggest that using a time-varying MLD does not significantly affect the simulated near-inertial current. Based on Alford (2003a), the spectral domain response function, $R \equiv \frac{Z(\sigma)}{T(\sigma)}$, can be written as,

$$R(\sigma) = \frac{1}{H}\frac{(r - i(f + \sigma))}{r^2 + (f + \sigma)^2}, \tag{3}$$

As $r << f$, the response function is strongly peaked around $\sigma = -f$, corresponding to a resonance between the near-inertial current and near-inertial wind forcing. The near-inertial wind power input (WPI) then can be computed as,

$$WPI_I = Re\{Z \cdot T^*\} = \frac{1}{H}\frac{r}{r^2 + (f + \sigma)^2}|T|^2, \tag{4}$$

Since $\mathrm{WPI_I}$ are strongly peaked at $\sigma = -f$ (anticyclonic), it then indicates that the $\mathrm{WPI_I}$ is linearly proportional to the clockwise (CW) rotating near-inertial wind stress variance.

2.3 Ocean Model and Experiments

The regional ocean modeling system (ROMS) developed by Rutgers University is used to simulate NIOs under realistic oceanic settings. ROMS is a free-surface, terrain-following, primitive-equation model based on hydrostatic and Boussinesq approximations (Shchepetkin and McWilliams 2005). It is designed to explicitly simulate regional oceanic circulations with high-horizontal resolutions. Physics parameterizations adopted in the ROMS include a KPP (K-profile parameterization, Large et al. 1994) vertical turbulent mixing closure scheme, a bi-harmonic horizontal Smagorinsky mixing for momentum, and a Laplacian horizontal mixing for tracer diffusion. The simulation domain covers the entire Gulf of Mexico (98–77°W and 18–33°N) with a 3 km horizontal resolution. The vertical grid has 60 levels with at least 20 levels in the upper 100 m to resolve the vertical structure of NI motions.

A series of experiments were performed by configuring ROMS with the same surface-atmosphere conditions except the surface wind forcing, which was computed from different reanalysis products to compare the diurnal winds represented by different datasets to observe and evaluate its impact on NI wave simulations. All other atmospheric variables required for computing surface momentum fluxes and surface heat fluxes were obtained from the ERAi, and the initial and boundary conditions for ROMS were derived from HYCOM GOM analysis (HYCOM expt 31.0). Because of the initial and boundary condition and the importance of the MLD, the simulated mean MLD is used to validate the model performance. As such, the simulated mean MLD is

in good agreement with that derived from HYCOM (not shown) and believe the model simulation outputs are trustable. Another point we would like to address here is that we use ERAi as a reference dataset in the model comparison section in this study. This is because 1) ERAi is the standard dataset operated by ECMWF, and 2) the CCMP wind analysis uses the ERA-Interim reanalysis winds as a first guess to find a best-fit solution to all of the available observations, including the inter-calibrated satellite data from numerous radiometers and scatterometers and in-situ data from moored buoys.

The Experiment runs, such as CCMP, MERRA, NCEP2, NARR, and NAM, are named by the surface wind products that applied. Simulations forced by various wind products were carried for one summer season (May–Sept) because the strongest LSB is occurred during summer (Zhang et al. 2009). Moreover, sea surface salinity was restored to its climatological value (CARS2009, Ridgway et al. 2002) to account for the river discharge effect that is not included in the ROMS simulations. Model outputs were archived every 3 h for analyses. Notice here we had chosen the year 2010 for the numerical experiments to compare with the observation. Year 2010 is a special year for the Gulf of Mexico because of the Deepwater Horizon Oil Spill event. Deepwater Horizon located at 28.74°N and 88.37°W, which is located at Mississippi Canyon. The oil spill event began on 20 April 2010 and was declared sealed on 19 September 2010. The entire period overlapped with the entire lifetime of the boreal summer near-inertial oscillation phenomena, so these phenomena have the potential triggers the vertical mixing in the surface water as well as the ocean interior.

Following Jing et al. (2015), the NI motion is analyzed based on the variance of the anti-cyclonically rotating currents with a frequency between 0.8 f and 1.2 f where f denotes the local inertial frequency. A slight modification of the lower and upper bounds does not have any significant impact on the major conclusions in this study. We focus on anti-cyclonically rotating variance because it is a key feature of near-inertial motions.

3 Results

3.1 Analysis of the Representation of LSB in Various Wind Products

As described in the introduction, the continental shelf in the Northern Gulf of Mexico is located along the critical latitude (30°N) where local Coriolis frequency is equal to diurnal frequency. Also, due to the Coriolis effect, wind vectors associated with the LSB are expected to rotate the clockwise (anticyclonic direction) during the day (Haurwitz 1947; Neumann, 1984; Abatan et al. 2014), which is in the same direction as the inertial oscillation in the ocean. For these two reasons, when investigating the resonated NI waves by land-sea breeze (LSB) circulation, it is always separated the clockwise and counter-clockwise rotations of winds. To do so, we applied rotary spectrum analysis here. Because of Coriolis effect, wind vectors associated with the LSB are expected to rotate clockwise (anticyclonic direction) during the course of the day (Haurwitz 1947; Neumann 1984; Abatan et al. 2014), which is in the same direction as the inertial oscillation in the ocean.

Figure 1 shows the domain averaged rotary spectrum of winds in the northern Gulf of Mexico (26°N to 30°N) derived from various wind products. The rotary spectrum analysis decomposes wind spectra into the clockwise and counter-clockwise component. From Fig. 1, it is evident that the clockwise component exhibits a much more pronounced peak near -1 cpd (cycle per day) (referred to as CW henceforth) than the counter-clockwise component (near 1 cpd, referred to as CCW henceforth), consistent with the LSB circulation. As f value varies from 0.88 (cycle per day) to 1 cpd between 26°N and 30°N, there is a significant overlap between diurnal frequency and inertial frequency band. It is expected that within this region resonant response of near-inertial oscillations to LSB can occur.

Despite that the inertial peaks are evident in all the wind products, their amplitude varies significantly. For the CW peak, the largest amplitude is given by NCEP2 and reaches 1×103 m^2 s^{-1}, which is more than 1.5 times the value of MERRA and ERAi. In contrast, NARR produces the largest amplitude for the CCW peak, whereas the smallest amplitude is given by MERRA. Therefore, different wind products differ not only in the intensity of LSB but also in its polarization.

We further compare diurnal wind ellipses computed from various wind products to those of buoy observations during the summer of 2010. A Butterworth band-pass (0.8–1.2 cpd) filter (Zhang et al. 2009) was first applied to the wind data at each station to extract the wind signal within the diurnal band. Then this bandpass filtered wind was subject to a harmonic analysis to estimate the phase and the amplitude of both zonal and meridional wind components. The size of the wind ellipse measures the amplitude of LSB while the shape of the ellipse reflects the polarization of LSB. For example, if the eccentricity of the ellipse is closed to zero (i.e., a circular shape), it means that the wind vector of LSB is isotropic with equal significance for u and v wind components and rotates like a circle with time. In contract, if the eccentricity is closed to unity, it means the LSB blows back and forth in a certain direction. As an example, if the ellipse is elongated in the south-north direction, it means the v-wind component is dominant with an insignificant u-wind component. The solid red triangle represents the synoptic snapshot of diurnal

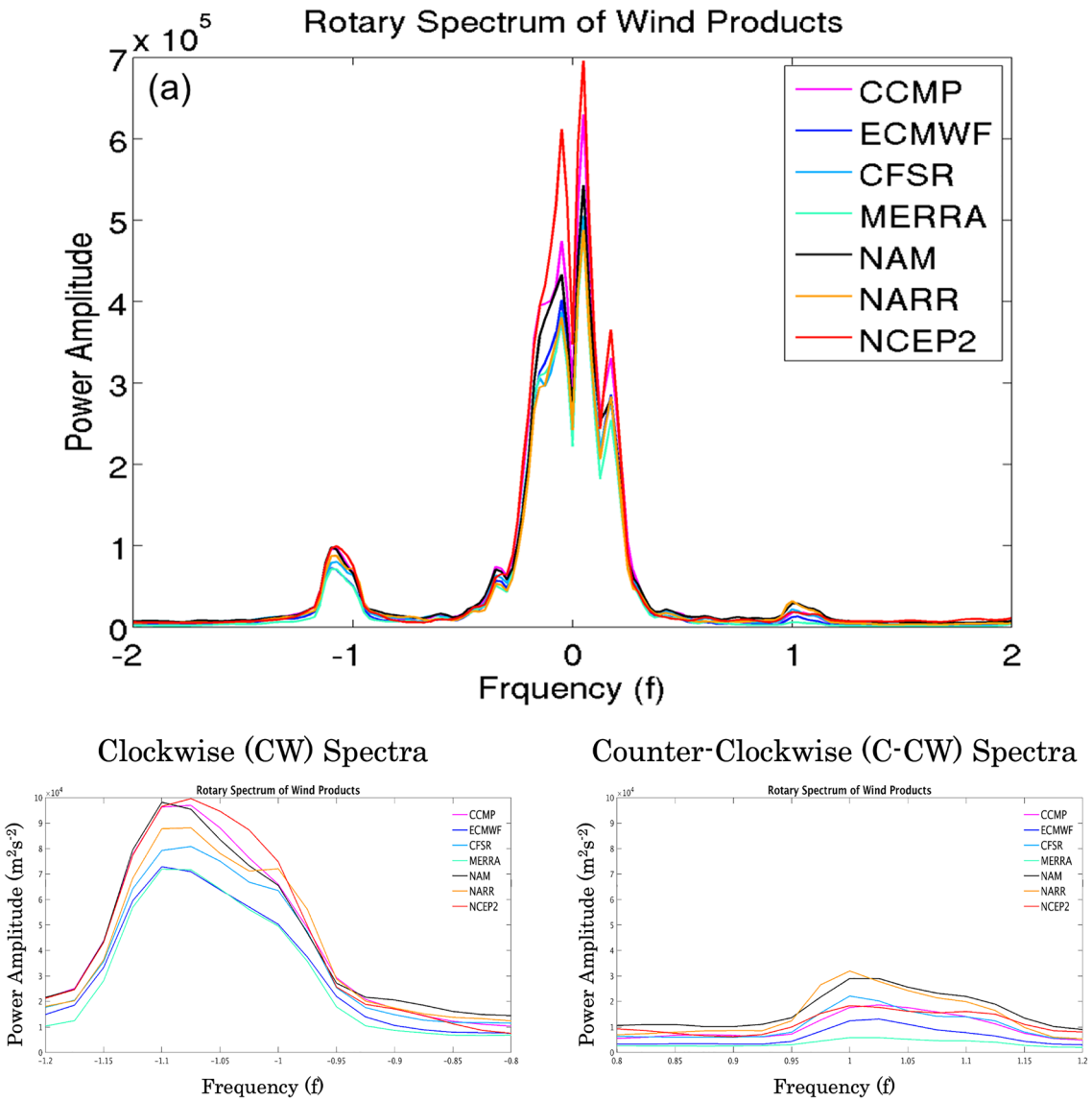

Fig. 1 Domain averaged rotary spectrum of surface winds among various wind products (colors) in the northern Gulf of Mexico (26°N–30°N) respecting by Coriolis frequency (**a**). Lower-left panel (**b**) shows the frequency limitation between from − 1.2 *f* to − 0.8 *f* for the clockwise rotation surface winds and lower right panel (**c**) shows the frequency limitation between 0.8 *f* and 1.2 *f* for the counterclockwise rotation surface winds on the lower-left panel

wind vectors at 1900 local time at each ellipse, indicating the phase information of the diurnal winds.

Figure 2 displays the wind ellipses computed from the various wind products and the buoy observations. The magnitude of the diurnal winds located on the Texas-Louisiana Shelf (TLS) from the reanalysis products are quite close to the buoy winds. The largest difference in diurnal wind amplitudes between reanalysis products and buoy observations occurs on the northeastern coastal of the Gulf of Mexico, where the intensity of the diurnal winds from all the reanalysis products is systematically underestimated by 58–75% compared to that of the buoy observations. This means that the current reanalysis/analysis wind products cannot well resolve the diurnal wind patterns, especially in the Northern East Gulf of Mexico, i.e., the western shore of Florida. The potential causes of these discrepancies are many, including but not only the temporal resolution, spatial resolution, and spatial resolution associated with the shape and the location of land/sea boundary within the model, the choice of Planetary Boundary Layer Parameterization Schemes, and so on. Although the exact reason behind these discrepancies is unknown, one major possible reason may be related to the relatively low horizontal resolutions of the wind products (Kara et al. 2008). Because wind speeds are

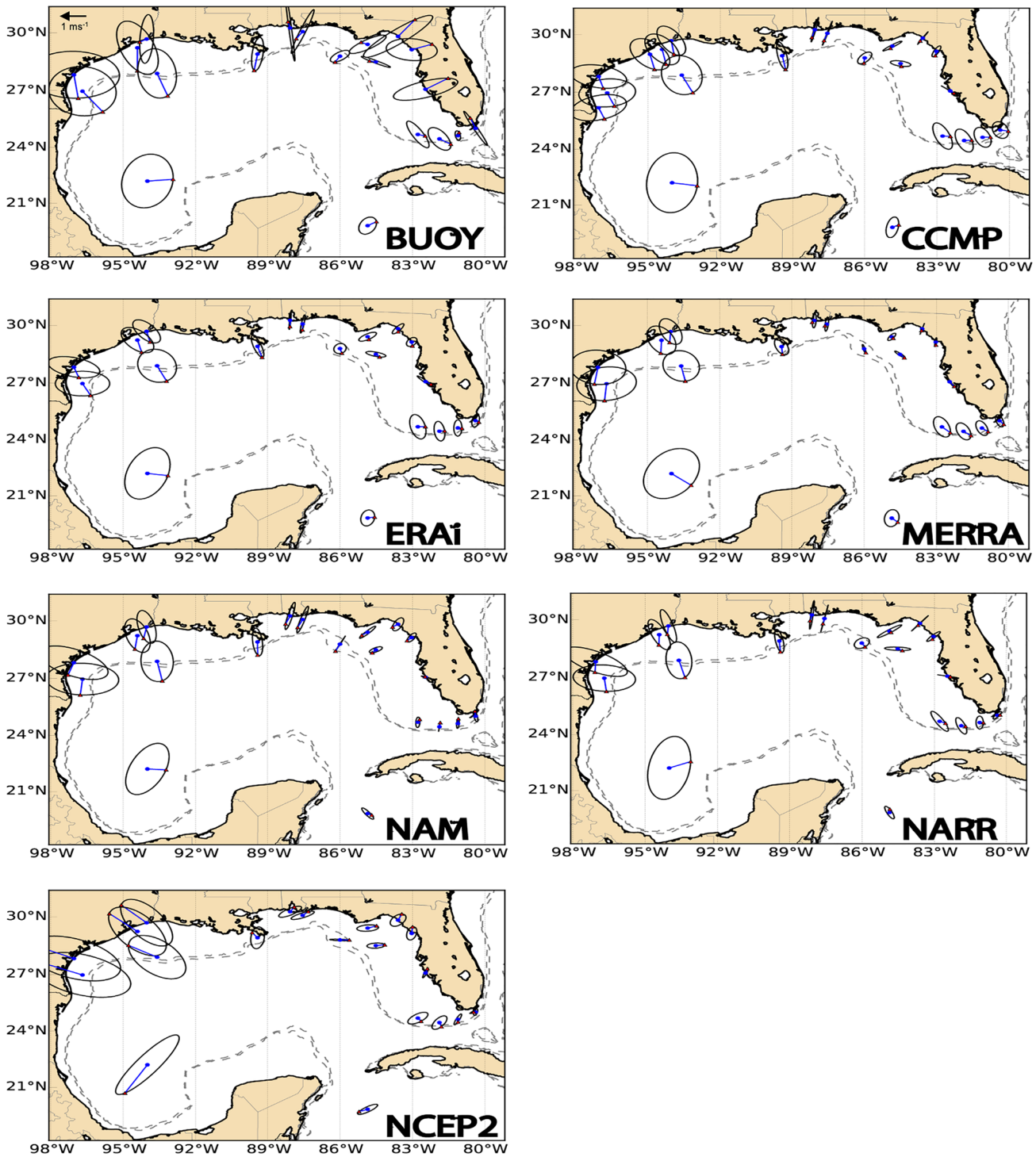

Fig. 2 Near-diurnal (between 0.8 and 1.2 cpd) surface wind ellipse harmonic analysis from buoy measurement (**a**), CCMP (**b**), ERAi (**c**), MERRA (**d**), NAM (**e**), NARR (**f**), and NCEP2 (**g**). The ellipses are derived by data on the duration of May-15 2010–Sept-15 2010. For each panel, the vectors show the wind direction of land-sea breeze at 1900 local time, and the size of the ellipse shows its strength

uniformly gridded, the coarse spatial grids near the land-sea boundaries may have difficulties to properly distinguish the values between ocean and land. This is so-called "land-contaminated" ocean-only winds or "ocean-contaminated" land-only winds, and typically depends on the extent of the land-sea mask.

To further quantify the difference between the observations and simulated wind products, we introduce three Root-Mean-Square-Error (RMSE) functions defined as:

$$\mathrm{RMSE}_{CW} = \sqrt{\frac{\sum_{n=1}^{n}\left(V_{\mathrm{windcw}} - V_{\mathrm{buoycw}}\right)^2}{n}}, \tag{5}$$

$$\mathrm{RMSE}_{CCW} = \sqrt{\frac{\sum_{n=1}^{n}\left(V_{\mathrm{windccw}} - V_{\mathrm{buoyccw}}\right)^2}{n}}, \tag{6}$$

$$\mathrm{RMSE}_{R} = \sqrt{\frac{\sum_{n=1}^{n}\left(R_{\mathrm{wind}} - R_{\mathrm{buoy}}\right)^2}{n}}. \tag{7}$$

where n is the number of the buoy stations, $V_{\mathrm{CW}}{}^2$ and $V_{\mathrm{CCW}}{}^2$ are the CW and CCW rotating wind variance in the diurnal band, and R is the ratio of V_{CW} to V_{CCW}. The subscript buoy and wind denote the values computed from the buoy and wind products, respectively. Equations 5 and 6 compute the RMSE for the CW and CCW rotating diurnal wind amplitude, respectively. Equation 7 computes the RMSE for the ratio of CW to CCW rotating diurnal wind amplitudes and provides a measurement for the difference of polarization between the observations and reanalysis wind products. Note that only Eq. 5 is relevant to the NI wind power and wind-generated NI kinetic energy in the ocean as only the CW rotating NI winds can resonate with NI waves in the ocean. The results from Eq. 5 to Eq. 7 are summarized in Table 2a. By comparing with observation, it is clear that in comparing CW rotating winds, the CCMP and NCEP2 have the smallest RMSE while ERAi, NAM, and NARR are at the same level. Surprisingly, the MERRA has the worst representation of CW rotating winds. Regarding the CCW rotating winds, CCMP, ERAi, NAM, and NARR are at the same simulation skill level as the lowest RMSE. The difference in CW rotating winds, although NCEP2 has the best CW rotating representation skills, the CCW representation skill is worse than the other products but better than MERRA. CW/CCW ratio RMSE can be represented as the simulation skill of diurnal winds. In this comparison, NCEP2 has the best representation skill, MERRA is the next. NAM and NARR are at the same level, and CCMP and ERAi belong to the worst case. The NCEP2 has the best simulation skills by comparing with other comparisons of wind products, although it still has an issue in representing CCW rotating winds. CCMP has better CW rotating wind magnitude and the CCW; the ratio of CW/CCW indicates it does not well represent the amplitude of diurnal winds. Overall speaking, if we only consider the diurnal winds, the NCEP2 is the best wind product in this comparison, even though it cannot represent the CCW rotating winds well. MERRA has good representation skills in CW/CCW ratio; however, because it has the worst RMSE in CW and CCW rotating winds (i.e., smallest amplitude, Fig. 2), we believe it is the last product to choose considering the diurnal winds. Note that the slab ocean model shows that only the CW rotating winds can resonate with NI waves in the ocean. Such a conclusion is relevant to Eq. 5. Therefore, we think the NCEP2 and CCMP are the first and second wind products to consider when investigating the diurnal wind-driven NI waves, while the MERRA is the last.

3.2 The Impact of Different Wind Products on the Simulated NIWs

In this section, we investigate the sensitivity of near-inertial wave response to diurnal wind variability in the northern Gulf of Mexico during summer using the framework of a realistic ocean model—ROMS. Figure 3 shows the spatial distribution of the summer-mean NI Wind Power Input (WPI)—the dot product of wind stress and surface velocity vector—simulated by ROMS forced by wind stresses from various wind products in 2010. The similarities are quantified using pattern correlation in reference to ERAi (Table 2b). The ERAi and CCMP have the highest correlation, probably because CCMP was produced by the same

Table 2 Comparable information among numerical experiments. (a) Root-Mean-Square Error for power amplitude of wind ellipse between buoy measurement and wind products. (b) Sum of the near-inertial WPI, among wind products over the northern Gulf of Mexico, and their pat-tern correlation. The contribution of near-inertial WPI in total WPI is showing in percentage in total WPI

	CCMP	ERAi	NAM	NARR	MERRA	NCEP2
Power amplitude integral RMSE (CW)	0.578	0.698	0.660	0.671	0.717	0.552
Power amplitude integral RMSE (CCW)	0.005	0.005	0.005	0.004	0.577	0.395
CW/CCW RMSE (CW)	1.075	1.013	0.459	0.493	0.016	0.005
	CCMP	ERAi	NAM	NARR	MERRA	NCEP2
Total near-inertial wind power input (TW)	5.20E-04	3.60E-03	4.20E-04	4.60E-04	2.80E-04	4.20E-04
Percentage in total WPI	5%	9%	5%	10%	8%	3%
Pattern correlation (WPI)	0.904	1.000	0.745	0.828	0.883	0.740

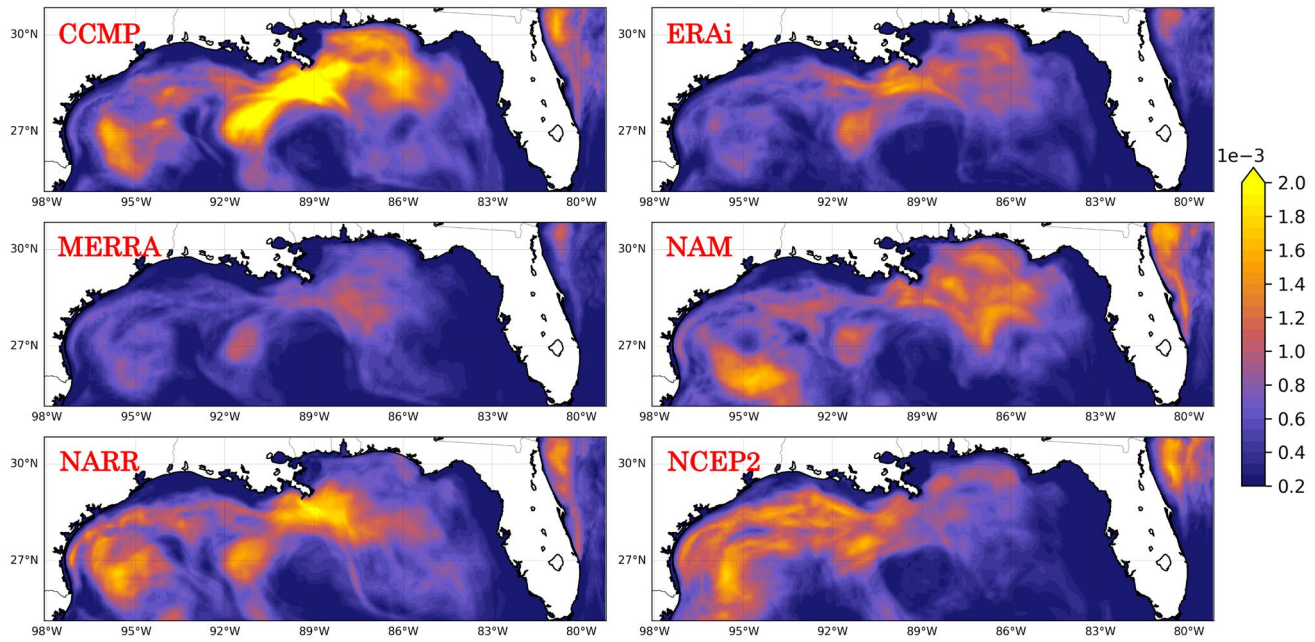

Fig. 3 Difference in simulated near-inertial wind power input among experiments over the North Gulf of Mexico (25°N above). From upper to lower and from left to right is CCMP, ERAi, MERRA, NAM, NARR, NCEP2, respectively

modeling system as the ERA product with an advanced satellite surface wind assimilation scheme. In contrast, NAM and NCEP2 produced the lowest pattern correlation value of ~ 0.74.

Although the spatial patterns of wind power derived from various wind products are similar (As shown in Fig. 3, in all cases, high values of WPI are concentrated along the northern coast of the Gulf of Mexico (26°N and above) and spread mostly over the continental shelf with the maximum located near the Mississippi Delta-Atchafalaya Bay), their magnitudes differ significantly. This is because that the uncertainties of the diurnal winds existed among wind products. For example, CCMP produced the strongest WPI with a maximum value reaching 2.0×10^{-3} Wm^{-2} near the Mississippi-Atchafalaya River plume region between 26–30°N and 92–88°W. Some high values of WPI are also found in the northeastern Gulf just offshore of St. Joseph Bay (~ 84°W) and in the northwestern Gulf near the Texas Shelf. Similar patterns of WPI can be found in ERAi NARR, and MERRA, but the magnitude is weaker by at least 50%. The magnitudes of WPI in NARR and NAM are quite similar, but the highest value of WPI in NARR only occurs near the Mississippi River bight, while in NAM the highest WPI value up to 1.5×10^{-3} Wm^{-2} occurs in the western Gulf between 25–27°N and 96–93°W with a second peak in the region between 27–30°N and 89–85°W. Unlike others, high WPI values in NCEP2 spread mostly over the entire Texas-Louisiana Shelf. The spatial distribution of the maximum WPI located near the Mississippi Delta-Atchafalaya Bay is because the MLD at this region is shallower. This can be explained by the theoretical analytic equations of the slab ocean model. In the slab ocean model, the near-inertial WPI is proportional to the reverse of the mixed layer depth (i.e., 1/H). In reality, during the summer period, the Mississippi-Atchafalaya River carries a significant amount of freshwater into the northern Gulf of Mexico, resulting in the shallow and stable MLD. Thus, although the amplitude of diurnal winds in another region like the Texas-Louisiana Shelf is much stronger than the Mississippi Delta-Atchafalaya Bay, the near-inertial WPI is still higher in the Mississippi Delta-Atchafalaya Bay region.

According to Furuichi et al. (2008) and Zhai et al. (2009), a majority (75–85%) of the WPI to near-inertial motions is dissipated within the upper ocean owing to enhanced vertical shear at the base of the mixed layer. This dissipated near-inertial wave energy is likely to contribute strongly to vertical mixing at the mixed-layer base. To examine how different wind products may affect mixing processes within the mixed layer, we integrated the near-inertial shear variance from surface to 50 m ($S^2 = \int_{50m}^{0} [(\partial u_i/\partial z)^2 + (\partial v_i/\partial z)^2] dz$) in each of the ROMS experiments. The subscript i indicates the near-inertial mode. The 50 m-depth is chosen because the summer MLD is typically shallower than 50 m. The results are shown in Fig. 4. Strong similarities among the experiments are clearly observed that there is a general agreement between shear variance and wind power. For example, high values of vertically integrated near-inertial shear variance up to 1.0×10^{-2} ms^{-2} are found along the northern Gulf of

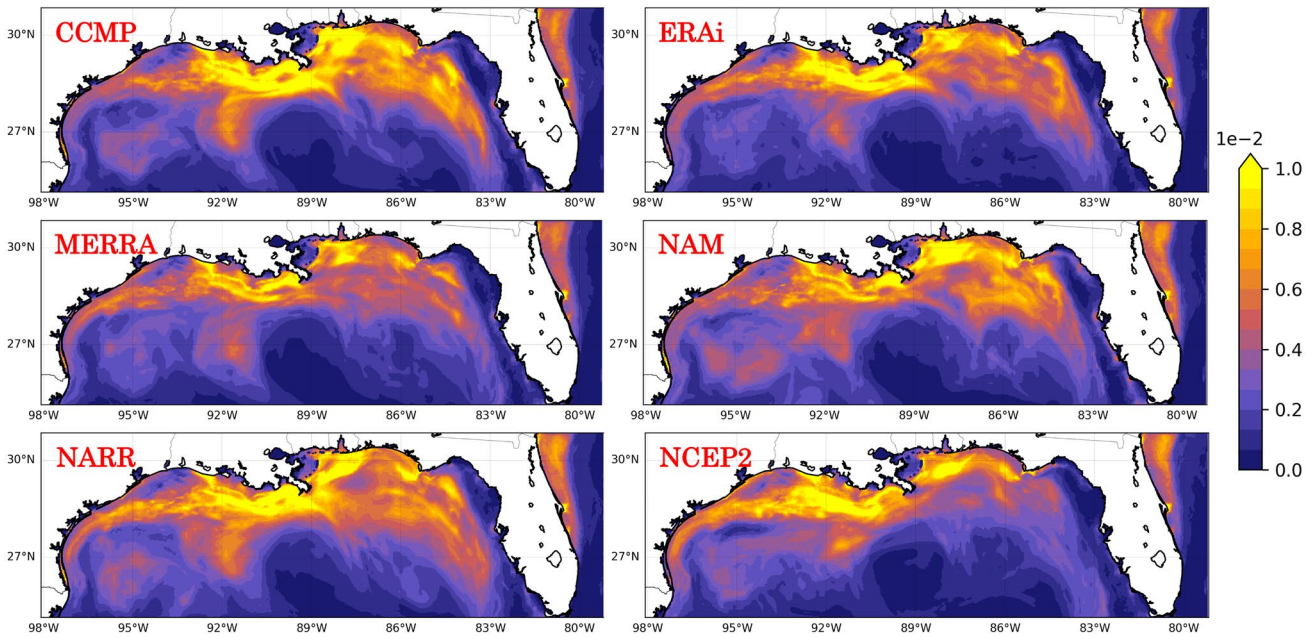

Fig. 4 Similar with Fig. 3, but for Spatial distribution of simulated near-inertial vertical shear variance integral from ocean surface to 50 m depth over North Gulf of Mexico

Mexico near the Mississippi-Atchafalaya River plume region where high WPI is also found. Consistent with WPI, the weakest shear variance is found in the MERRA simulation, where has the weakest diurnal wind forcing. Typical orders of shear variance within the mixed layer in our numerical experiment during summer are between 10^{-4} and 10^{-6} s^{-2}. The maximum shear variance along the northern Gulf of Mexico is found near the Mississippi Delta-Atchafalaya Bay in the ROMS experiments with values approaching 2×10^{-4} s^{-2}. It suggests that the existence of NI waves may contribute to the deepening of the bottom depth of the mixed layer in that region.

4 Summary and Discussion

In this study, we show that there are significant differences in the currently available reanalysis wind products in representing diurnal wind variability along the northern Gulf coast where LSB circulation dominates during summer. By validating simulated winds to in situ buoy observations, we are able to identify biases in the reanalysis winds. One of the major biases is that all the reanalyzed winds systematically underestimate the diurnal wind variation in the northeastern Gulf of Mexico off the western Florida shelf. Given the broad shelf of the region, the bias in reanalysis winds can lead to significant errors in simulating near-inertial motions in the ocean if they are used to construct ocean model forcing fields, such as COREII (Coordinated Ocean Research Experiments version 2 Large and Yeager 2009). The cause of this bias in reanalysis winds is not clear. Although some possibilities are addressed before, further studies are required to investigate this issue.

We then examine the sensitivity of near-inertial response of the ocean to various reanalysis wind products by conducting a set of high-resolution ROMS simulations. Using these simulations, we explore relationships between near-inertial WPI and diurnal wind variability in different wind products, respectively. The simulation results show high values of WPI along the northern Gulf coast, particularly near the Mississippi Delta-Atchafalaya Bay—a finding that supports the dominance of NI resonant response to diurnal winds in the region. Moreover, the simulations show a significant sensitivity of NI WPI in the northern Gulf region to various wind products. The strongest intensity of the WPI is found using CCMP winds, whereas the weakest is MERRA. We further examine the near-inertial shear variance in ROMS simulations. Our simulation results show a high value of the shear variance along the northern Gulf of Mexico and reveal a close correspondence between the shear variance and the wind power and the diurnal wind variability. These results support the notion that stronger diurnal winds lead to a stronger resonant response of NI motions that in turn produce a stronger shear variance in the upper ocean. Our approach is motivated by previous research (Simpson et al. 2002; Zhang et al. 2009) finding that the near-inertial motions within the northern Gulf are results of resonant response to diurnal wind variations due to the strong LSB

circulation in the region and demonstrated that NI waves are considered an important contributing factor to vertical mixing within the mixed layer.

Major conclusions from this part of the study are as follows: (1) Reanalysis winds consistently underestimate diurnal wind variability in the northern Gulf, particularly in the western Florida Shelf. (2) Among all the reanalysis wind products, the coarse resolution NCEP2 gives the best agreement with observed buoy winds while the high-resolution MERRA product has the worst agreement. (3) By using near-inertial WPI to gauge near-inertial motions, we show that in ROMS simulations high values of WPI are consistently found in the northern Gulf coast, particularly near the Mississippi-Atchafalaya River plume region—a result that supports the dominance of near-inertial resonant response to diurnal winds in the region. (4) There is a significant sensitivity of near-inertial WPI in the northern Gulf region to various wind products. The strongest intensity of the WPI is obtained by using CCMP winds, while the weakest is obtained by MERRA. (5) Uing ROMS simulations, we further computed the near-inertial vertical shear-variance to investigate the vertical mixing at the mixed-layer base caused by near-inertial waves and its sensitivity to diurnal wind forcing in the northern Gulf region. Previous studies reason that near-inertial motions can enhance vertical mixing, causing mixed layer to deepen. As such, near-inertial waves are thought to be an important factor contributing to vertical mixing within the mixed layer. Our simulation results do show that the most of high values of the shear variance are located on the northern Gulf of Mexico and the stronger shear variance does correspond to wind products that have stronger diurnal wind variability (e.g., CCMP). These results are consistent with the spatial distribution of the WPI, supporting the notion that stronger diurnal winds lead to stronger resonant response of near-inertial motions that in turn produce a stronger shear variance in the upper ocean.

An important point that we want to discuss here is that all the ROMS sensitivity experiments were conducted by replacing entire wind forcing using various reanalysis products (Table 2b). Therefore, it is difficult to relate the simulated MLD directly to diurnal winds and NIWs, because the MLD is affected by not only diurnal winds and NIWs, but also low-frequency winds. One way to isolate the effect due to uncertainties in the diurnal winds is to conduct a set of sensitivity experiments similar to the one described here except that only the diurnal component of the winds is altered. We suggest future studies should explore this aspect.

Acknowledgements This project would not have been possible without funding from the Gulf of Mexico Integrated Spill Response Consortium (Grant Number: M1400397) and EPSCOR (Established Program to Stimulate Competitive Research) in Rhode Island, provided by the National Science Foundation (award no. OIA-1655221). We acknowledge the U.S. National Data Buoy Center for providing a security in-situ buoy dataset and Dr. Jaison Kurian to assist ROMS configuration for this study. We also thank the Texas A&M University High-Performance Research Computing group for their outstanding computing support. Especially thank the valuable contributions from Dr. Matthew Howard and share this publication to heaven.

References

Abatan AA, Abiodun BJ, Omotosho BJ (2014) On the characteristics of sea breeze over Nigerian coastal region. Theor Appl Climatol 116:93–102. https://doi.org/10.1007/s00704-013-0931-z

Alford MH (2003a) Improved global maps and 54-years history of wind-work on ocean inertial motions. Geophys Res Lett 30:1424. https://doi.org/10.1029/2002GL016614

Alford MH (2003b) Redistribution of energy available for ocean mixing by long-range propagation of internal waves. Nature 423:159–162. https://doi.org/10.1038/nature01628

Atlas R, Hoffman RN, Ardizzone J, Leidner SM, Jusem JS, Smith DK, Gombos D (2011) A cross-calibrated multiplatform ocean surface wind velocity product for meteorological and oceanographic applications. Bull Amer Meteor Soc 92:157–174. https://doi.org/10.1175/2010BAMS2946.1

Cardona Y, Bracco A (2016) Predictability of mesoscale circulation throughout the water column in the Gulf of Mexico. Deep-Sea Res II 129:332–349. https://doi.org/10.1016/j.dsr2.2014.01.008

Craig PD (1989a) Constant eddy-viscosity models of vertical structure forced by periodic winds. Cont Shelf Res 9:343–358. https://doi.org/10.1016/0278-4343(89)90038-1

Craig PD (1989b) A model of diurnally forced vertical current structure near 30° latitude. Cont Shelf Res 9:965–980. https://doi.org/10.1016/0278-4343(89)90002-2

D'Asaro EA (1985) The energy flux from the wind to near-inertial motions in the surface mixed layer. J Phys Oceanogr 15:1043–1059. https://doi.org/10.1175/1520-0485(1985)015%3c1043:TEFFTW%3e2.0.CO;2

Dee DP, Uppala SM, Simmons AJ, Berrisford P, Poli P, Kobayashi S, Andrae U, Balmaseda MA, Balsamo G, Bauer P, Bechtold P, Beljaars ACM, Van De Berg L, Bidlot J, Bormann N, Delsol C, Dragani R, Fuentes M, Geer AJ, Haimberger L, Healy SB, Hersbach H, Hólm EV, Isaksen L, Kållberg P, Köhler M, Matricardi M, Mcnally AP, Monge-Sanz BM, Morcrette J-J, Park B-K, Peubey C, De Rosnay P, Tavolato C, Thépaut J-N, Vitart F (2011) The ERA-interim reanalysis: configuration and performance of the data assimilation system. Q J Roy Meteor Soc 137(656):553–597. https://doi.org/10.1002/qj.828

Edwards CR (2008) Coastal ocean response to near-resonant sea breeze/land breeze near the critical latitude in the Georgia Bight. Carol Digital Repos. https://doi.org/10.17615/9jxw-wk30

Feng Y, Fennel K, Jackson GA, DiMarco SF, Hetland RD (2014) A model study of the response of hypoxia to upwelling-favorable wind on the northern Gulf of Mexico shelf. J Mar Syst 131:63–73. https://doi.org/10.1016/j.jmarsys.2013.11.009

Furuichi N, Hibiya T, Niwa Y (2008) Model-predicted distribution of wind-induced internal wave energy in the world's oceans. J Geophys Res 113:C09034. https://doi.org/10.1029/2008JC004768

Haurwitz B (1947) Comments on the sea-breeze circulation. J Meteor 4:1–8. https://doi.org/10.1175/1520-0469(1947)004%3c0001:COTSBC%3e2.0.CO;2

Hunter E, Chant R, Bowers L, Glenn S, Kohut J (2007) Spatial and temporal variability of diurnal wind forcing in the coastal ocean. Geophys Res Lett 34(3):L03607. https://doi.org/10.1029/2006gl028945

Hyder P, Simpson JH, Xing J, Gille ST (2011) Observations over an annual cycle and simulations of wind-forced oscillations near the critical latitude for diurnal-inertial resonance. Cont Shelf Res 31:1576–1591. https://doi.org/10.1016/j.csr.2011.06.001

Jiang J, Lu Y, Perrie W (2005) Estimating the energy flux from the wind to ocean inertial motions: the sensitivity to surface wind fields. Geophys Res Lett 32:L15610. https://doi.org/10.1029/2005GL023289

Jing Z, Chang P, DiMarco SF, Wu L (2015) Role of near-inertial internal waves in subthermocline diapycnal mixing in the northern Gulf of Mexico. J Phys Oceanogr 45:3137–3154. https://doi.org/10.1175/JPO-D-14-0227.1

Jochum M, Briegleb BP, Danabsoglu G, Large WG, Norton NJ, Jayne SR, Alford MH, Bryan FO (2013) The impact of oceanic near-inertial waves on climate. J Clim 26:2833–2844. https://doi.org/10.1175/JCLI-D-12-00181.1

Kanamitsu M, Ebisuzaki W, Woollen J, Yang SK, Hnilo JJ, Fiorino M, Potter GL (2002) NCEP/DOE AMIP-II reanalysis (R-2). B Am Meteorol Soc 83:1631–1643. https://doi.org/10.1175/BAMS-83-11-1631

Kara AB, Wallcraft A, Barron CN, Hurlburt HE, Bourassa MA (2008) Accuracy of 10 m winds from satellites and NWP products near land-sea boundaries. Geophy Res 113:C10020. https://doi.org/10.1029/2007JC004516

Klein P, Lapeyre G, Large WG (2004) Wind ringing of the ocean in presence of mesoscale eddies. Geophys Res Lett 31:L15306. https://doi.org/10.1029/2004GL020274

Large WG, Pond S (1981) Open Ocean momentum flux measurements in moderate to strong winds. J Phys Oceanogr 11:324–336. https://doi.org/10.1175/1520-0485(1981)011%3c0324:OOMFMI%3e2.0.CO;2

Large WG, Yeager SG (2009) The global climatology of an interannually varying air–sea flux data set. Clim Dyn 33:341–364. https://doi.org/10.1007/s00382-008-0441-3

Large WG, McWilliams JC, Doney SC (1994) Oceanic vertical mixing—a review and a model with a nonlocal boundary-layer parameterization. Rev Geophys 32:363–403. https://doi.org/10.1029/2004GL020274

Mesinger F, Dimego G, Kalnay E, Mitchell K, Shafran PC, Ebisuzaki W, Jović D, Woollen J, Rogers E, Berbery EH, Ek MB, Fan Y, Grumbine R, Higgins W, Li H, Lin Y, Manikin G, Parrish D, Shi W (2006) North American regional reanalysis. B Am Meteorol Soc 87(3):343–360. https://doi.org/10.1175/bams-87-3-343

Mickett JB, Serra YL, Cronin MF, Alford MH (2010) Resonant forcing of mixed layer inertial motions by atmospheric easterly waves in the northeast tropical Pacific. J Phys Oceanogr 40:401–416. https://doi.org/10.1175/2009JPO4276.1

Morey SL, Zavala-Hidalgo J, O'Brien J (2005) The seasonal variability of continental shelf circulation in the northern and western Gulf of Mexico from a high-resolution numerical model. In: Sturges W, Lugo-Fernandez A (eds) Circulation in the Gulf of Mexico: observations and models, vol 161. American Geophysical Union, Washington DC, pp 203–218. https://doi.org/10.1029/161GM16

Munk W (1980) Internal waves and small-scale processes. In: Warren BA, Wunsch C (eds) Evolution of physical oceanography. MIT Press, pp 264–291

Nam S, Send U (2013) Resonant diurnal oscillations and mean alongshore flows driven by sea/land breeze forcing in the coastal Southern California Bight. J Phys Oceanogr 43(3):616–630. https://doi.org/10.1175/JPO-D-11-0148.1

Neumann J (1984) The coriolis force in relation to the sea and land breezes—a historical note. B Am Meteorol Soc 65:24–26. https://doi.org/10.1175/1520-0477(1984)065%3c0024:TCFIRT%3e2.0.CO;2

Pollard RT, Millard RC (1970) Comparison between observed and simulated wind-generated inertial oscillations. Deep-Sea Res 17:153–175. https://doi.org/10.1016/0011-7471(70)90043-4

Ridgway KR, Dunn JR, Wilkin JL (2002) Ocean interpolation by four-dimensional least squares—application to the waters around Australia. J Atmos Ocean Technol 19:1357–1375. https://doi.org/10.1175/1520-0426(2002)019%3c1357:OIBFDW%3e2.0.CO;2

Rienecker MM, Suarez MJ, Gelaro R, Todling R, Bacmeister J, Liu E, Bosilovich MG, Schubert SD, Takacs L, Kim G-K, Bloom S, Chen J, Collins D, Conaty A, Silva AD, Gu W, Joiner J, Koster RD, Lucchesi R, Molod A, Owens T, Pawson S, Pegion P, Redder CR, Reichle R, Robertson FR, Ruddick AG, Sienkiewicz M, Woollen J (2011) MERRA: NASA's modern-era retrospective analysis for research and applications. J Clim 24(14):3624–3648. https://doi.org/10.1175/jcli-d-11-00015.1

Rimac A, Von Storch JS, Eden C, Haak H (2013) The influence of high-resolution wind stress field on the power input to near-inertial motions in the ocean. Geophys Res Lett 40:4882–4886. https://doi.org/10.1002/grl.50929

Rippeth TP, Simpson JH, Player RJ, Garcia M (2002) Current oscillations in the diurnal-inertial band on the Catalonian shelf in spring. Cont Shelf Res 22:247–265. https://doi.org/10.1016/S0278-4343(01)00056-5

Rogers E, DiMego G, Black T, Ek M, Ferrier B, Gayno G, Janjic Z, Lin Y, Pyle M, Wong V, Wu W-S (2009) The NCEP North American Mesoscale modeling system: recent changes and future plans. In: 23rd Conference on weather analysis and forecasting/19th conference on numerical weather prediction, Omaha, 1–5 June 2009

Saha S, Moorthi S, Pan H-L, Wu X, Wang J, Nadiga S, Tripp P, Kistler R, Woollen J, Behringer D, Liu H, Stokes D, Grumbine R, Gayno G, Wang J, Hou Y-T, Chuang H-Y, Juang H-MH, Sela J, Iredell M, Treadon R, Kleist D, Delst PV, Keyser D, Derber J, Ek M, Meng J, Wei H, Yang R, Lord S, Dool HVD, Kumar A, Wang W, Long C, Chelliah M, Xue Y, Huang B, Schemm J-K, Ebisuzaki W, Lin R, Xie P, Chen M, Zhou WH, Zou C-Z, Liu Q, Chen Y, Han Y, Lidia Cucurull S, Reynolds RW, Rutledge G, Goldberg M (2010) The NCEP climate forecast system reanalysis. B Am Meteorol Soc 91(8):1015–1058. https://doi.org/10.1175/2010bams3001.1

Simpson JH, Rippeth TP, Hyder P, Luca IM (2002) Forced oscillations near the critical latitude of diurnal-inertial resonance. J Phys Oceanogr 22:177–187

Shchepetkin AF, McWilliams JC (2005) The regional oceanic modeling system (ROMS): a split-explicit, free-surface, topography-following-coordinate oceanic model. Ocean Model 9:347–404. https://doi.org/10.1016/j.ocemod.2004.08.002

Teague WJ, Wijesekera HW, Jarosz E, Lugo-Fernandez A, Hallock ZR (2014) Wavelet analysis of near-inertial currents at the East Flower Garden Bank. Cont Shelf Res 88:47–60. https://doi.org/10.1016/j.csr.2014.06.013

Von Storch JS, Sasaki H, Marotzke J (2007) Wind-generated power input to the deep ocean: an estimate using a 1/10° general circulation model. J Phys Oceanogr 37:657–672. https://doi.org/10.1175/JPO3001.1

Von Storch JS, Eden C, Fast I, Haak H, Hernandez-Deckers D, Maier-Reimer E, Marotzke J, Stammer D (2012) An estimate of the Lorenz energy cycle for the world ocean based on the 1/10° storm/ncep simulation. J Phys Oceanogr 42:2185–2205. https://doi.org/10.1175/JPO-D-12-079.1

Watanabe M, Hibiya T (2002) Global estimates of the wind-induced energy flux to inertial motions in the surface mixed layer. Geophys Res Lett 29:L1239. https://doi.org/10.1029/2001GL014422

Wunsch C (1998) The work done by the wind on the oceanic general circulation. J Phys Oceaogr 28:2332–2340. https://doi.org/10.1175/1520-0485(1998)028%3c2332:TWDBTW%3e2.0.CO;2

Xu FH, Chang YL, Oey LY, Hamilton P (2013) Loop current growth and eddy shedding using models and observations: analysis of the July 2011 eddy-shedding event. J Phys Oceanogr 43:1015–1027. https://doi.org/10.1175/JPO-D-12-0138.1

Zavala-Hidalgo J, Morey SL, O'Brien JJ (2003) Seasonal circulation on the western shelf of the Gulf of Mexico using a high-resolution numerical model. J Geophys Res 108:3389. https://doi.org/10.1029/2003JC001879

Zhai X, Greatbatch RJ, Eden C, Hibiya T (2009) On the loss of wind-induced near-inertial energy to turbulent mixing in the upper ocean. J Phys Oceanogr 39:3040–3045. https://doi.org/10.1175/2009JPO4259.1

Zhang Z, Hetland RD (2012) A numerical study on convergence of alongshore flows over the Texas-Louisiana shelf. J Phys Oceanogr 117:C11010. https://doi.org/10.1029/2012JC008145

Zhang X, DiMarco SF, Smith DC, Howard MK IV, Jochens AE, Hetland RD (2009) Near-resonant ocean response to sea breeze on a stratified continental shelf. J Phys Oceanogr 39:2137–2155. https://doi.org/10.1175/2009JPO4054.1